# Sensor Management for Space-Based Sensing Constellations

**Joshua Davis, T Jennings-Bramly, J Symons, F Waltho**
*Defence Science and Technology Laboratory, UK*

## ABSTRACT

Space-based sensing is likely to increase in prevalence in the coming years, yet challenges still exist from a sensor management perspective. To address this we use modelling, simulation and optimisation to quantify the possible Space Domain Awareness (SDA) opportunities (or threats) and in doing so propose methods to potentially improve space-based sensing capability. At scale, we model and simulate Resident Space Object (RSO) population scenarios to investigate the feasibility of space-to-space observation opportunities and any dependency on a sensor's orbital placement and manoeuvring dynamics. We then move on to apply optimisation routines to construct constellation solutions for space-based sensors that maximise the total number of observation opportunites and coverage for a given RSO target population of interest. These constellation solutions are then used to analyse the feasibility of multi-orbit missions that can in principle achieve similar coverage results by manoeuvring to all the orbits in the constellation over the space-based sensor's lifetime. Optimal sequencing of these selected orbital transfers is achieved by posing as a Travelling Salesman Problem which minimises the total velocity change (dV) to visit all orbits once. We end by demonstrsating the analyisis of the close approaches experienced in a low-thrust electric propulsion (EP) transfer to Geosynchronous Earth Orbit (GEO), obtained by fitting a Q-Law model to the Two-Line Element set history of Northrup Grumman's second Mission Extension Vehicle (MEV-2).

## 1 INTRODUCTION

The growth of emerging new space mission types (e.g. active debris removal, in-orbit servicing, satellite inspection), the associated advancements in spacecraft control and propulsion technologies, and the ever-growing list of space-faring actors have all contributed to making space an increasingly complex and diverse operational domain. These factors, as well as the continued proliferation of space debris and other hazards to spaceflight safety, highlight and underline the importance of improved Space Domain Awareness (SDA) capabilities, in both traditional and novel sensing paradigms.

The application of space-based sensing for SDA is witnessing growing interest regarding its strengths in tackling these new space challenges and facilitating assured and timely action in the increasingly diverse operational landscape. The choice of orbital elements for the space-based sensors in a constellation is an analogous problem to the optimisation of the geographic distribution of a sensor network. Space-based sensor modelling requires slightly different approaches to the ground-based equivalent, but the overall output objective of maximizing observation opportunities are similar. In this study, we aim to produce a similar evaluation to ground-based sensor networks but across space-based sensor systems.

In this work, the objective of the space-based SDA sensors in the LEO scenarios is to perform the following functions: catalogue maintenance and resolved imaging. Our chosen primary metric of performance is the number of close approaches within a certain detectability distance threshold which we have assumed is required to provide sufficient angular resolution for resolved imaging. Resolved imagery would be useful for a number of characterisation purposes including investigation of anomalies and capability assessment. For the deep-space scenario (4), our objective is instead focussed towards analysing the threat landscape via observation window assessment (analogous to satellite overflight warning), during a Geostationary Transfer Orbit (GTO) to GEO (GTO-GEO) low thrust transfer orbit of a high mass satellite.

We present a toolbox of modelling, simulation and optimisation techniques to explore some questions of particular interest related to the scenarios identified:

- How important is orbit selection for a space-based sensor?
- How can a constellation of space-based sensors be assessed and selected?

- What is the feasibility of undertaking a multi-orbit mission to visit N orbits with good space-based sensing opportunities?
- If a space-based sensor has low-thrust electric propulsion (EP) capability, traversing over a long period of time a large swathe of orbital regimes, how does this affect the statistics of SDA opportunities and/or threat windows?

The methods proposed herein could be applied to many scenarios, for the purposes of this paper we've chosen to focus on the following representative scenarios:

1. Single orbit; non-manoeurving; LEO;
2. Constellation; non-maneouvring; LEO;
3. Single; chemical manoeuvring; LEO;
4. Low thrust continuous transfer orbit; GTO-GEO.

We begin by giving a short overview of the technical methods used and the performance metrics pertaining to SDA capabilities of a space-based sensor. We then show results from assessing the performance of a variety of orbital configurations against a simulated space object population. Subsequently, we apply a well-known Time to Close Approach (TCA) algorithm to efficiently assess the close approach statistics. In particular, we identified the orbital regions from which a space-based sensor performs best against our SDA opportunity evalutation criteria, and also the feasibility of these close approaches in terms of the amount of time the observer and target are within a given detectability range. These results are then used to formulate a subset selection problem which is solved using two methods: a brute force Monte Carlo simulation and a Non-Selective Dominating Genetic Algorithm (NSGA-II) as a multi-objective optimiser. The results give a proof of concept methodology for generating candidate space-based sensing constellations in the polar LEO region.

We then investigate the feasibility of a single space-based sensor with manoeuvring capability performing a multi-orbit mission. We do this by re-posing the constellation solutions as a multiple-orbit mission and calculating the velocity change (or dV) requirements to visit all orbits once. Here, we use three standard orbit transfer models: single revolution Lambert RPO, Hohmann and Bielliptic. Other methods exist, however, these three models are among the most well known and simplest, and hence are appropriate for the proof of concept developed herein. The optimum sequencing of orbit transitions is obtained by solving a Travelling Salesman problem using a Genetic Algorithm (GA). These results give insight into the viability of multiple-orbit missions of this type and how other types of missions can be produced with the tools developed.

Our final application applies the TCA algorithm to a special ephemeris of interest, taken to be a continuous low-thrust EP transfer from an initial highly elliptic transfer orbit to GEO. For the purposes of this work, MEV-2 was studied, as it was a recent case of interest. We assess the potential observation windows (SDA opportunity/threat) over the long timespan of the transfer through the different orbit regimes, and also provide preliminary results on an investigation into the feasibility of being subject to nefarious circumnavigation operations (chaser spacecraft circumnavigates in close proximity around the target spacecraft) at the end phase of the GTO to GEO transfer.

## 2 TECHNICAL APPROACH

### 2.1 System Overview

In Fig. 1 we provide an overview of the inputs, methods and outputs for the close approach assessment tool developed, forming the basis of the analysis in this paper. The blocks in Fig. 1 will be introduced in the following sub-sections.

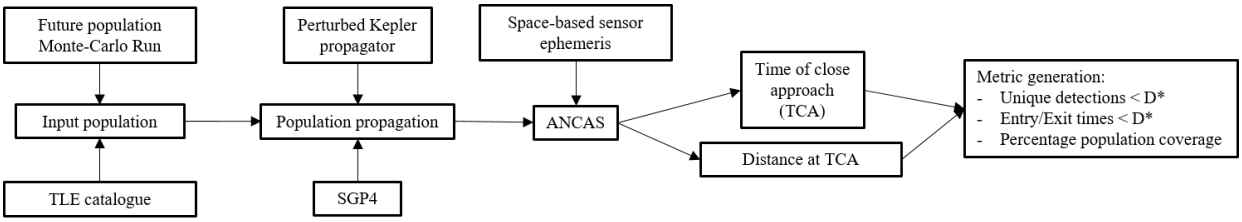


*Fig. 1: Close approach assessment toolbox*

### 2.2 Population Progagation

The Future Populations dataset was produced from DAMAGE, a model that was developed in partnership with the University of Southampton and GMV Innovating Solutions Limited. DAMAGE was verified against the European Space Agency (ESA) MASTER future population model and uses MASTER 2018 population as the initial population for the model. DAMAGE incorporates future trends in orbital element distributions derived from historic data analysis, launch traffic schedule, estimates for mega constellation growth and catastrophic collision events. In this study to reduce computational burden, an arbitrarysingle realisation of a Monte Carlo simulation of this model for 2022 was selected[1]. Further work, could reproduce the analysis herein on further realisations to produce averaged results. It is comprised of 95293 RSO objects with predicted keplerian orbital elements, mass, diameter, object status, country of origin and object type, we use these variables to select subset populations of interest. In this paper, results are produced for three population scenarios (see Table 1).

We use a perturbed Keplerian propagator with secular gravity and drag to propagate the subset population's Keplerian orbital elements [1]. Our reasoning for using this simplified model as opposed to the usual SGP4 propagator was to make the dynamics consistent with our manoeuvre models and to enable us to initialise directly from the Future Population dataset without introducing additional uncertainty by converting to a TLE.

| scenario | eccentricity | perigee (km) | mass (kg) | owner | target population size | debris | simulation time (days) |
|---|---|---|---|---|---|---|---|
| 1 | e <0.5 | p < 8300 | m>4 | allied | 2267 | no | 1 |
| 2 | e<0.9 | p > 1000 | m>4 | all | 10010 | no | 153 |

*Table 1: Population scenarios filtered from 2022 Future Population Monte Carlo simulation dataset.*

### 2.3 Time to Closest Approach (TCA)

The Time of Closest Approach (TCA) and the associated distance between pairs of orbiting objects is an important calculation in SDA. It forms the first step in estimating an object's likelihood of collision [1]. However, it is also useful in flagging the time opportunities when objects are within a given relative distance threshold, D*, such that

[1] Monte Carlo simulations of Future populations are also available for 2032 and 2042, but not considered in this study. 

suitable space-based observations can be made. Alternatively, to indicate the times when an object is under threat of a close range detection, or from an unfriendly satellite payload.

The simplest method of calculating the TCA and relative distance is by brute force, where the two objects are propagated with very small time steps then explicitly taking all the times of local minima in relative euclidian distance over a given time interval. Here, the error of the TCA strongly depends on the size of the time step chosen. This approach is computationally intensive, rendering TCA calculations across a large population of space-objects unfeasible.

Due to the large scale of the tradespace, in this study we require an efficient means to calculate all the close approach times, $t_n^*$, for $\mathrm{t} \in [\mathrm{t}_0, \mathrm{t}_\mathrm{f}]$ such that $\mathrm{d}(t_n^*) < \mathrm{D}^*$. Therefore, we have decided to implement a commonly used method known as Alfano Negron Close Approach Software (ANCAS) [1, 2], which is widely known for its speed in estimating the TCA. It does, however, have some limitiations on the accuracy of solutions, but for the purposes of analysing the large scale statistics of close approaches across populations, we have deemed it sufficient for the purpose herein. Ideally, these results would act as a preliminary solution to then apply more accurate close approach algorithms, for example, therecent work by Denenberg, which has proven that similar speeds but with significant improvements in accuracy can be made [3, 4].

The ANCAS algorithm first defines a positive distance function

$$d(t) = (r_a(t) - r_b(t)) \cdot (r_a(t) - r_b(t)) = \xi(t) \cdot \xi(t) \qquad (1)$$

where $\xi(t)$ is the relative euclidian distance between two objects, *a* and *b*. The first and second order time derivatives of d(t)

$$\dot{d}(t) = 2\left(\dot{\xi}(t) \cdot \xi(t)\right) \qquad (2)$$

$$\ddot{d}(t) = 2\left(\ddot{\xi}(t) \cdot \xi(t) + \dot{\xi}(t) \cdot \dot{\xi}(t)\right) \qquad (3)$$

are made up of the relative velocity between the two objects state propagation and the associated relative acceleration components, which in this study is calculated up to the $J_2$ term. The condition for a local minima at time $\mathrm{t}_\mathrm{n}^*$ in terms of the distance functions is then

$$\dot{d}(t_n^*) = 0 \qquad (4)$$

$$\ddot{d}(t_n^*) > 0. \qquad (5)$$

The ANCAS approach constructs piecewise cubic splines scaled by a time interval $\Delta t = t_{i+1} - t_i$ such that the coefficients defined in terms of the distance function and its derivatives exactly represent the function at the boundaries

$$P_m(\tau) = \sum_{k=0}^{m} \alpha_k \tau^k \,, \qquad 0 \le \tau \le 1. \qquad (6)$$

An approximation for the TCA is then calculated by finding a root $\tau_n^*$ of $P_3(\tau)$ on the interval $0 \le \tau \le 1$. A simple check for the existence of real roots on the interval is first made to reduce unessessary function calls to the analytic expression for roots of a cubic polynomial. The ANCAS approximation for the TCA is then taken to be

$$t_n^* = t_i + \tau_n^* \Delta. \qquad (7)$$

### 2.4 Distance of Closest Approach (DCA)

The distance of closest approach, $d_n^*$, is calculated by forming a quintic spline for every *IJK*-component evaluated at $\tau_n^*$, this ensures that the acceleration terms are included and will improve the accuracy of the result. The ANCAS expression for $d_n^*$ is given by

$$d_n^* = \sqrt{P_{5\,I}^2(\tau_n^*) + P_{5\,J}^2(\tau_n^*) + P_{5\,K}^2(\tau_n^*)}\,. \tag{8}$$

### 2.5 Entry and Exit Times

An important consideration in assessing the feasibility of an SDA opportunity is the amount of time the two objects are within a distance threshold, D*. The value of D* will vary with the type of observation (/interaction) and the detection (/engagement) range of the satellite payload.

We calculate the times of entry and exit to the D* distance threshold by solving the following equation

$$\sqrt{d(t)} = D^*. \tag{9}$$

We use a Newton-Raphson root solver at multiple initialisations centred on $t_n^*$ until two unique solutions are found and take the difference to calculate the total interaction time window.

## 3 LEO SDA OPPORTUNITY METRICS

### 3.1 Orbit Performance Metrics

In this section we investigate how SDA opportunities vary with orbital placement of the space-based sensor. We have identified two key metrics to use within our assessment:

1. the total number of close approaches < D* over a given simulation time; and
2. the total number of unique targets <D* over a given simulation time.

A higher total number of close approaches is indicative of greater revisit rates, resulting in better quality tracking accuracy, or the ability to take observations across multiple viewing angles. Whereas higher unique detections indicates better overall coverage of the target population of interest, it is similar to a groundbased sensor having a larger Field of Regard (FoR) and is important if one wishes to build a diverse catalogue of observation data.

### 3.2 Orbital Assessment

Here we assess how the two performance metrics are influenced by the choice of orbital parameters for the space-based sensor. We limit this analysis to a variation across the inclination and semi-major axis variables, keeping all other orbital elements fixed. In Table 2 we set out the parameters for this particular case study. In order to achieve better resolution over an orbital regime of particular interest, herein we have opted to consider only a 60deg proportion of the possible orbital inclination range centred around polar orbits, and also semi-major axis between 6600km and 8000km. However, the algorithms can be applied to any orbital regime. The total gridsize represents the number of space-based orbits assessed, uniformly incremented over the inclination and semi-major axis ranges. Finally, we have assumed a 200 km distance threshold limit for collection of observation data on most target objects, to achieve a sufficient resolution to be of value. However, we note that this is an arbitrary choice and will depend heavily on the sensor system employed.

| Target Population (see Table 1) | D* | Inclination (deg) | Semi-major axis (km) | Total gridsize ($N_{grid}$) | Total simulation time |
|---|---|---|---|---|---|
| 1 | 200km | [60, 120] | [6600, 8000] | 6400 | 1 day |

*Table 2: Orbital assessment setup*

Fig. 2 shows 2D contour plots using a Delaunay triangulation algorithm to interpolate the gridpoint evaluations across the semi-major axis and inclination domain. Initially, we assumed these plots would closely correlate with the target populations density distribution across both inclination and semi-major axis variables. However, we see in Fig. 2(a) for the total close approaches metric, peaks centred at approximately (82deg, 6800km) and (82deg, 7100km). This contradicts this initial assumption for inclination, because by far the most significant peak (see Fig. 2c) in the target population's inclination distribution is at ~97deg, where the greatest number of LEO target orbits reside for this population scenario. We suspect what we are seeing is a reflection of the target population's inclination distribution at 90deg which marks the prograde-retrograde transition. This makes intuitive sense as there will be a greater number of retrograde polar orbits passing by a space-based sensor travelling in the opposite direction. There is, however, a strong correlation with respect to the semi-major axis variable, where we observe two large peaks in the population density of the target population (see Fig. 2d), matching the peaks in total close approaches in Fig. 2(a) at 6800km and 7100km.

In Fig. 2(b) we observe two distinct horizontal bands, in the contour plot for the unique SDA opportunities metric, matching the two peaks in the target populations semi-major axis density distribution. This suggests there is a clear

correlation across the semi-major axis variable but not for inclination with regards to the unique SDA opportunities metric.

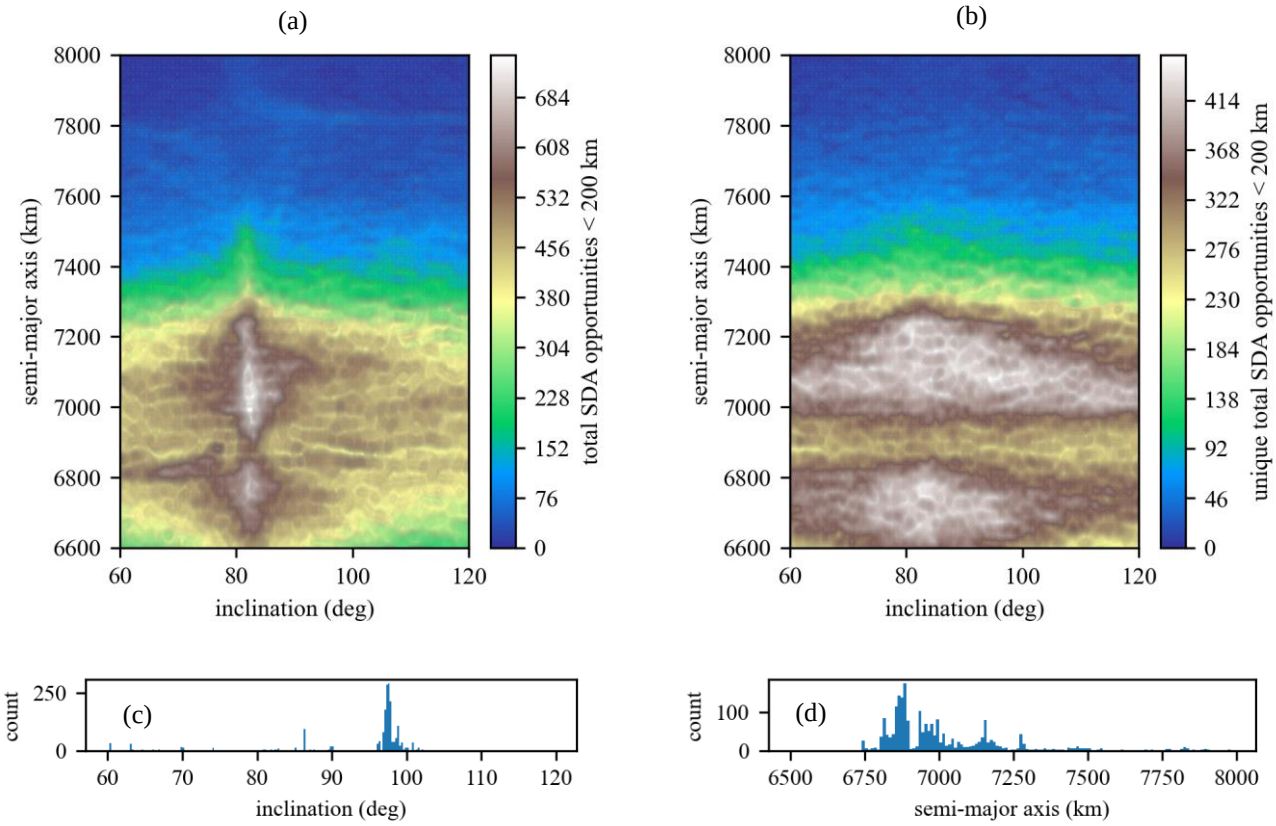


*Fig. 2: Population scenario 1, interpolated contour plots depicting (a) total number of SDA opportunities (b) total number of unique satellites detected in 1 day with D* = 200km (c) target population scenario 1 inclination distribution (d) semi-major axis distribution*

### 3.3 Feasibility of SDA Opportunites

The close approaches <D* calculated by ANCAS and described in the previous section constitute a generous definition of an SDA opportunity because they omit the amount of time an object is within the detectability range, D*. Herein, for simplicity, we omit the distinction between detectability and resolvability due to the strong dependence on the sensor system and the size of the target object involved. However, the combination of target range and detectability time will determine the type of SDA opportunity available.. For example, a very short time window at a large range would probably render detailed imagery unworkable but could be enough to perform a state vector update. Furthermore, the uncertainty of the target object's state vector has not been taken into account. If the state vector of the target object has not been updated recently, the volume describing the positional uncertainty in the close approach calculation could well be comparable to, if not greater than, the volume of the detectability zone governed by the intersection of the target's trajectory with the space-based sensor's moving detectability sphere (radius D*). More work is needed to properly represent the positional uncertainty of the target with the feasibility of the SDA opportunity in terms of probability. Although these details haven't been accounted for, the calculation of the entry and exit times gives some indication of the volume of this detectability zone on a population level. This enables us to examine the proportion of close approaches that are likely to be unfeasible from a sensor management perspective.

To reduce computational burden, a downselection of the orbits from scenario 1 was used. For 500 randomly sampled space-based orbits in scenario 1, totalling 300000 close approaches, we calculate the detectability time by using the method describe in section 2.5 for D* = 200 km. In Fig. 3a and 3b we show how the relative difference in semi-major axis and inclination influences the detectability time statistics, respectively.

In Fig. 3c we plot the 2D density plot over the minimum close approach distance and the corresponding detectability time, where we detect a quadratic relation between these two variables. This effectively provides a lower bound for detectability time with close approach distance: for a close approach ~0km the minimum detectability time is ~25seconds, but diminishes to zero as the close approach distance tends towards D*. It should also be noted that the greatest density of close approaches lie on this bound, therefore if a sensor's minimum detectability time were to be above 25 seconds, the total number of SDA opportunities would fall sharply.

For optical sensors, the inclusion of illumination conditions is another necessary factor to consider and will inenvitably reduce the proportion of tenable SDA opportunities further. Work is currently being developed to investigate the relative significance of illumination, however, it is not considered here.

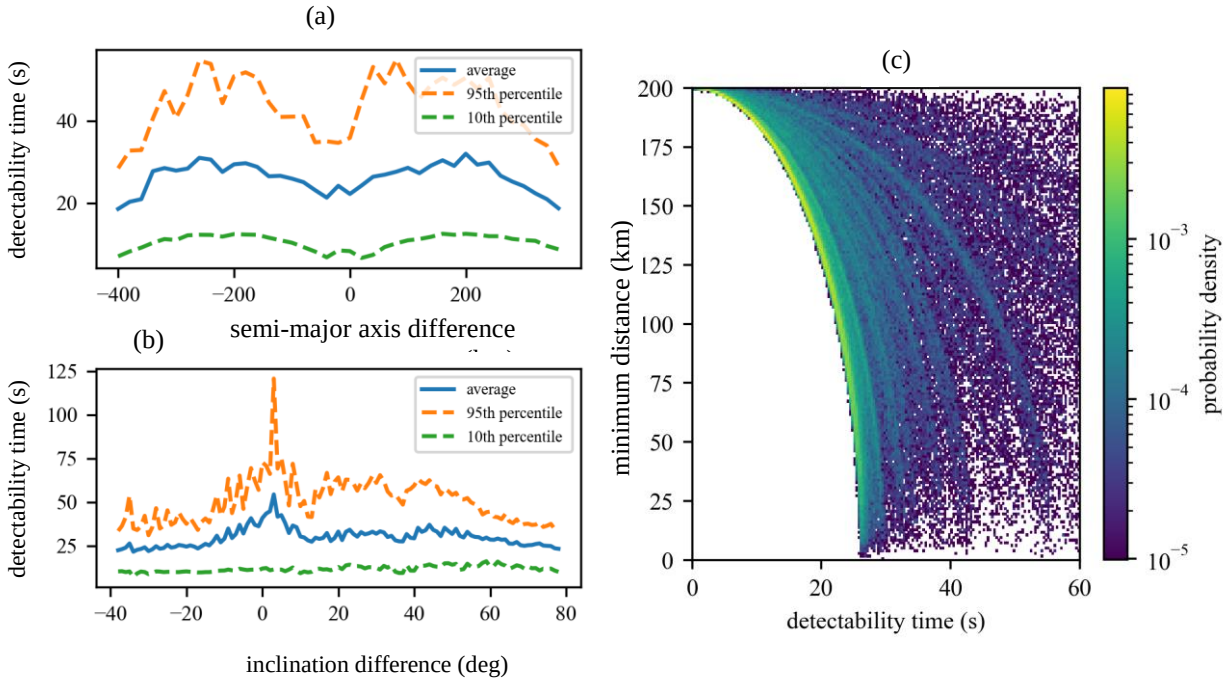


*Fig. 3: (a) detectability time variation with observer-target semi-major axis difference, (b) inclination difference, (c) 2D density plot of minimum distance with detectability time (300000 close approaches randomly sampled from Fig. 2)*

# 4 SPACE-BASED SENSOR CONSTELLATIONS

## 4.1 Objectives

The results from the orbital assessment study in section 3.2 provides a convenient read off of the expected performance metrics for a single space-based sensor orbit. We now utilise these results to investigate the expected performance of a constellation of *N* space-based sensors. In so doing we present a proof of concept method for designing a constellation of space-based sensors which aims to maximise the SDA opportunities which could then inform operators on how to most efficiently build a catalogue of resolved imagery and/or RSO state vectors.

The total number of opportunities is independent across the orbits so we are able to quickly compute the constellation equivelent by summing the *N* single orbit selections. To calculate the total unique number of satellites we must first manipulate the results into a binary matrix of size $Mgrid \times Mpop$, where $Mgrid$ is the number of space-based orbits evaluated in the inclination vs. semi-major axis grid, and $Mpop$ is the target population size. It is then possible to make *N* orbit selections and calculate the overall percentage coverage of the population. These two constellation performance metrics form a multi-objective problem to solve.

The performance metrics function $F$ takes a binary encoded variable $x$ of size $Mgrid \times 1$; a one indicates an orbit has been selected. The output of $F(x)$ is a $2 \times 1$ column vector $y$, with rows corresponding to the total number of SDA opportunities and percentage coverage. At this point it is possible to add scaling factor to incorporate the effective feasibility of the performance result. However, in this study we use the idealised results as shown in Fig. 2. We now have multi-objective optimisation problem to solve, taking the form

$$\min -F(x)$$

$$s.t \left( \sum_{n=1}^{M_{grid}} x_n - N \right)^2$$

where a constraint condition has been included to ensure that only *N* subset selections are made to form the solution.

## 4.2 Proof of Concept: Constellation Design

The simplest way of solving this multi-objective problem is by brute force Monte Carlo simulation, where a large number of random $x$ are generated and the best performing solutions are selected. However, as constellation size, *N*, increases, the number of ways to choose *N* satellite orbits out of the 6400 specified in Table 2 is given by the combinatorial binomial coefficient $C_N^{6400}$ making this approach to simulation less effective as *N* increases. For example, there are ~ 2 x $10^{86}$ ways of selecting a constellation composed of 32 satellites.

Another approach investigated here is using a NSGA-II [5] to generate a Pareto front of solutions [6]. The NSGA-II algorithm is a type of evolutionary algorithm customised for multi-objective problems; a random population of solutions is initially created, then each generation of solutions is sorted and compared by a metric known as the crowding distance. Best performing (or elite) solutions are permitted to carry on to the next generation, a subset undergo mating and the remainder are rejected. Upon each generation the Pareto front will tend towards the Pareto-optimal set of solutions.

In Fig. 4 we compare the results of the brute force Monte Carlo with 100,000 random samples of $x$ to the NSGA-II method with different population and generation sizes. We see that as the constellation size increases the NSGA-II pareto front of solutions outperforms the Monte-Carlo approach in both metrics, particularly in total SDA opportunities. In addition, we observe from the $N$ = 64 case that problem complexity is such that even after 1000 generations the pareto front has still not fully converged to a final state as seen for the smaller constellation size examples.

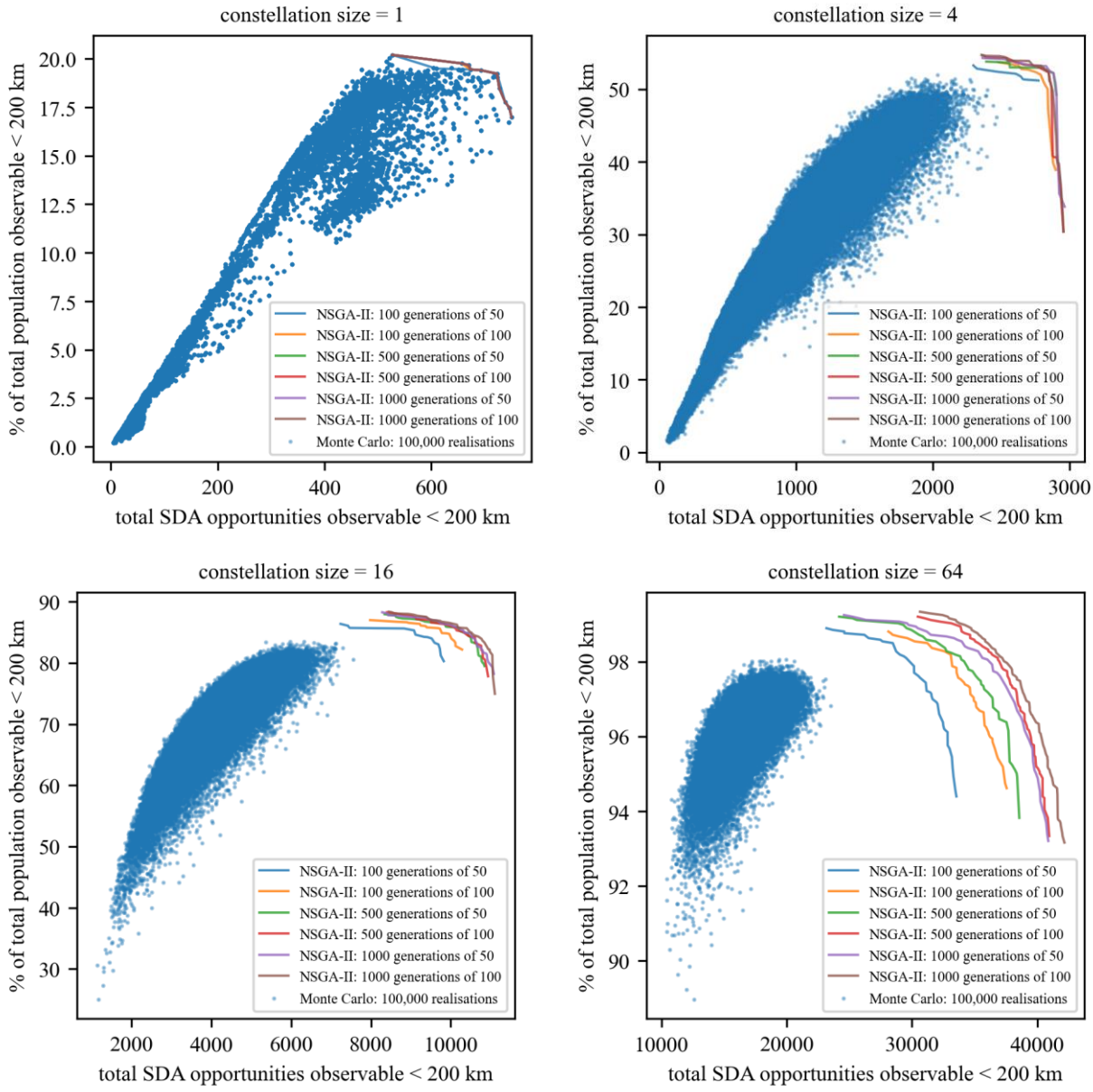


*Fig.4: Monte Carlo and NSGA-II method comparisons for proof of concept constellation design.*

This study highlights the importance in selecting appropriate orbits for a constellation in order to maximise the SDA objectives of the constellation operators. It can be seen from the Monte Carlo results that arbitrary orbit selections, particularly at low N, lead to a significant reduction of space-based sensor constellation performance.

Here, we have chosen a generic case but we note that this tool is able to construct objectives that maximise the number of detections for any subset population. One possible use case could apply to mega-constellation operators needing to know where to position a space-based sensor constellation tasked with perfoming regular health checks or anomaly detection on their assets. Another could be on how to minimise the time taken to build a full catalogue of imagery data to be used for SDA characterisation purposes.

# 5 MULTI-ORBIT MISSIONS

## 5.1 Travelling Salesman Problem

In the previous section we solved a multi-objective problem to obtain a Pareto set of optimal solutions to find all the best combinations of orbits to maximise population coverage and total opportunities. Here, we explore the possibility of visiting all those computed orbits making up the constellation with a single spacecraft with manoeuvring capability. In principle, this approach gives similar effective coverage to the constellation solution over the lifetime of the manoeuvring space-based sensor.

We are interested in finding the best performing sequence of transfers between the orbits contained in each constellation solution, such that all orbits are visited once and the combined velocity change, dV, for all transfers is minimised. This is a travelling salesman problem, but cast onto the inclination and altitude of orbits, as opposed to the traditional city to city time of travel or distance travelled formulation. To obtain solutions we use a Genetic Algorithm to find the optimal sequence of orbits to undertake. While this type of problem could be solved by brute force, a Genetic Algorithm is a reliable and more efficient solution for searching large solution spaces.

We consider three fundamental burn models for the orbit transitions:

- Direct single revolution solution of Lambert problem;
- Bielliptic; and
- Hohmann.

In the Lambert transfer case we select the minimum dV over a 500 minute time window sampled uniformly 100 times to obtain the transit time. The solution to the Lambert problem has a retrograde and prograde solution - the best performing is selected assuming a non-hit Earth condition is satisfied.

For the bielliptic transfer, since the semi-major axes and inclinations of the two orbits are known, a Nelder-Mead optimization procedure is applied to calculate the minimum dV over the three optimisation variables: the inclination change performed at the first burn, the inclination change performed at the second burn, and the bi-elliptic radius. The bi-elliptic radius is constrained to values less than 100,000 km to avoid impractical transfer times.

The Hohmann transfer is calculated similarly to the bielliptic transfer by applying a Nelder-Mead optimisation procedure to calculate the minimum dV. However, the Hohmann transfer is only optimized over two variables: the inclination change performed at the first burn, and the inclination change performed at the second burn.

For each burn model, we take the Pareto front constellation solutions computed in the previous section and construct a matrix $dV_{ij}$ of size $N \times N$. Each element in the matrix corresponds to the amount of dV required to transfer from the ith to jth orbit in the optimised constellation.

## 5.2 Travelling Salesman Problem Results

We now apply the GA travelling salesman solver to obtain the optimum sequence of transfers for each Pareto-optimal constellation solution with N = 9 orbits, where 9 is an arbitrary choice for demonstration purposes. The GA population size is 20, which was selected via trial and error to achieve computational efficiency. In this case the number of generations is variable, such that the algorithm will keep iterating until the last 50,000 generations show no improvement in performance. In Fig. 5, 6 and 7 we present results for each burn model: Direct Lambert, bielliptic and Hohmann respectively.

In Fig. 5(a-b), 6 (a-b) and 7 (a-b) we show the travelling salesman solutions on an arbitrary timeline to visualise the orbital transfers of a manoeuvring spacecraft visiting each orbit of the constellation once. These are shown in the semi-major axis (a) and inclination variables (b). In blue we plot the result corresponding to the constellation solution which requires the most total dV to visit all its orbits, and in orange we plot the constellation which requires the least in total

dV. We observe that across all the burn models the orbital diversity is greater in the semi-major axis for the most expensive in total dV orbital sequences, with semi-major axis between 6750km and 7025km. This is compared to a much smaller range of only 6900km to 7000km for the least expensive orbital sequences. Across inclination there is a maximum of 1.25deg inclination change across all orbits in the Pareto-optimal orbits selected, suggesting that the NSGA-II optimiser has converged to orbit solutions that are densely distributed around the local maxima at ~80deg inclination seen in Fig. 2a.

We can see from Fig. 5(c), 6 (c) and 7 (c), where we show for all 39 Pareto-optimal constellation solutions, the corresponding total dV required to visit all its orbits and the expected population coverage from doing so. Here we see that there is there is a sharp increase in total dV required to achieve greater than 75% population coverage for all burn models. Moreover, Fig. 5(d), 6 (d) and 7 (d), where we plot the Pareto-optimal constellation performance metrics with the marker of each solution scaled according to the computed total dV, we see a clear trade-off between population coverage and how much dV is required to traverse all orbits. Linking this back to the orbital timelines in 5(a-b), 6 (a-b) and 7 (a-b), as one would expect, the increase in orbital diversity improves population coverage but increases dV requirements. Whereas the decrease in orbital diversity over the semi-major axis means more SDA opportunities will be available overall, but at the cost of less total population coverage.

When comparing across the burn models, we have found that the Lambert transfer is considerably more expensive than the minimised Hohmann and bielliptic models; the total dV for the Lambert transfers ranges between 8.1 km/s and 38.7km/s, which likely renders this number of orbital transfers unfeasible. However, for Hohmann and bielliptic we see in 6 (c-d) and 7 (c-d) orbital sequences that have acceptable total dV between ~0.3km/s and 2 km/s, which only results in a small reduction in total population coverage compared to the best performing solution. We also note that the Hohmann and bielliptic models both give similar dV results.

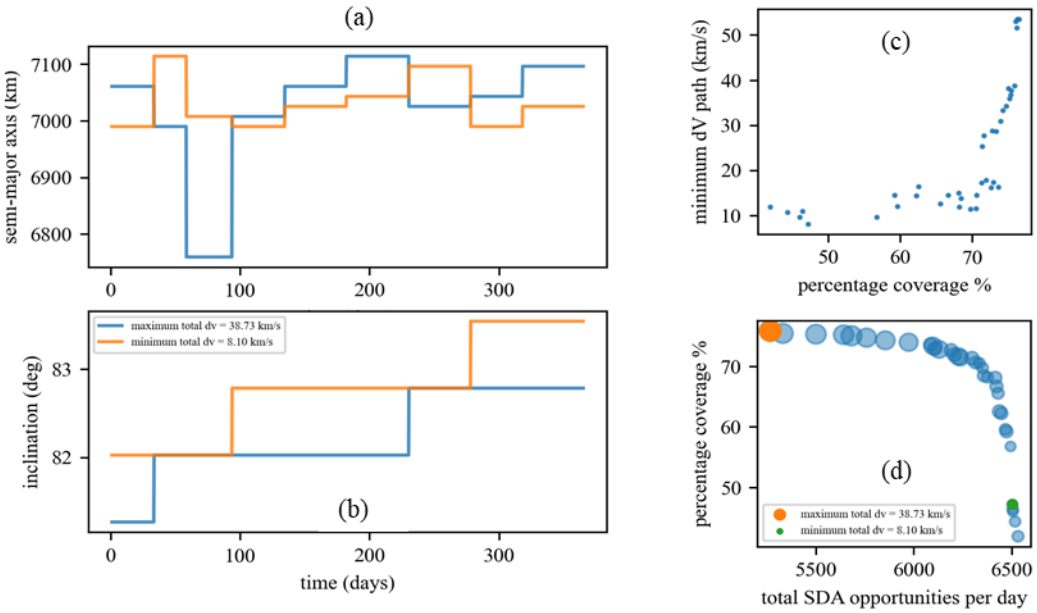


*Fig. 5: Direct Lambert burn model, Travelling Salesman solution, N = 9*

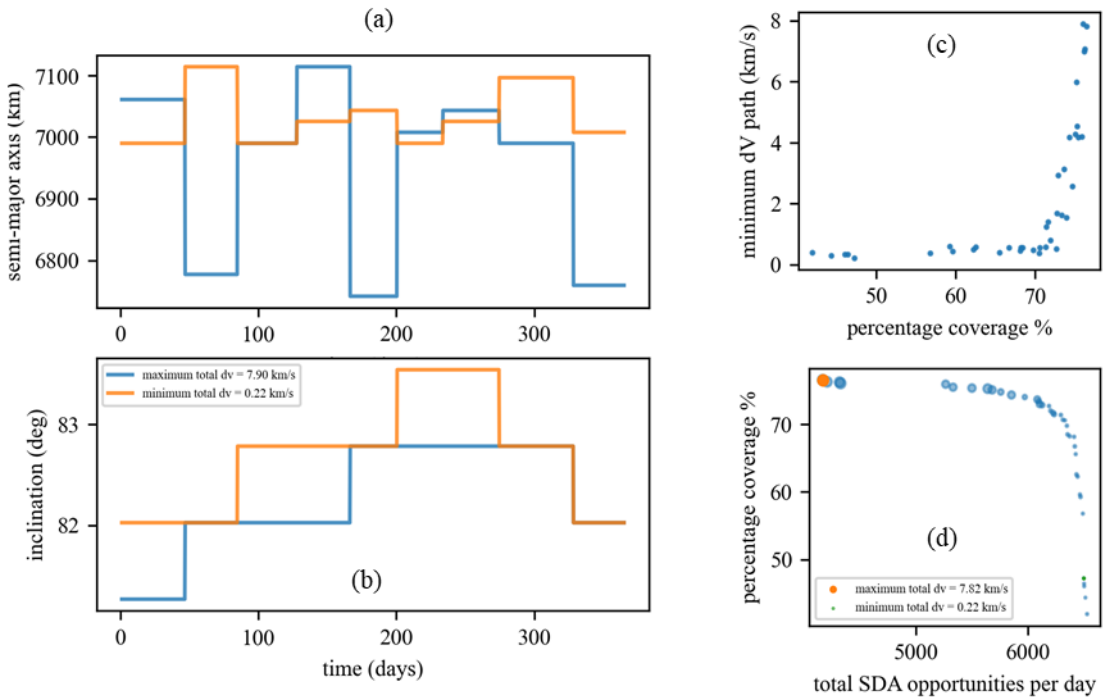


*Fig. 6: Bieliptic burn model Travelling Salesman solutions, N = 9*

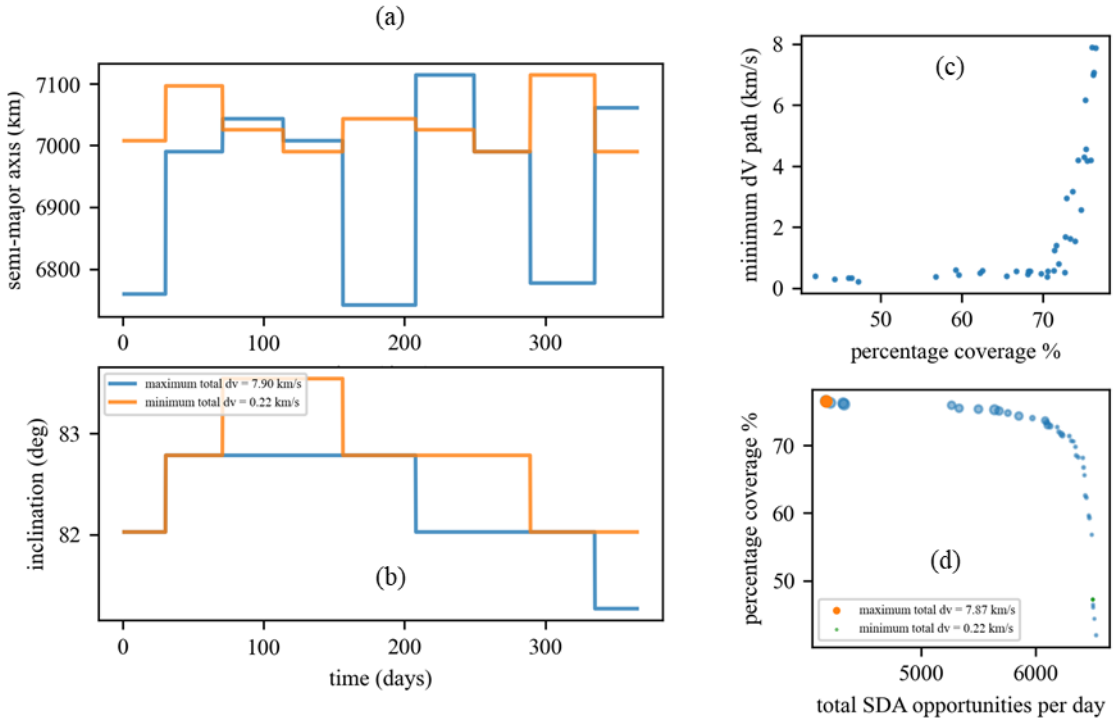


*Fig. 7: Hohmann burn model Travelling Salesman solutions, N = 9*

## 6 MEV-2 EP GTO-GEO TRANSFER

In this final piece of work we depart from solely LEO orbital regimes and apply ANCAS to the Mission Extension Vehicle 2 (MEV-2) mission undertaken by Northrop-Grumman. Observations of MEV-2 were collected by the Five Eyes community during a collaboration coined PHANTOM ECHOES [7] that enabled the testing of data assimilation/processing techniques and a variety of tracking and custody maintenance modalities. The mission provided a unique opportunity to observe a cooperative, low-thrust EP target during the GTO and close-approach phases before it docked with its target, Intelsat 10-02.

In this study, we explore the intermediate phase of the transfer from GTO to first arrival in GEO. Due to the continous low-thrust dynamics, the spacecraft will pass through a large swathe of orbital regimes. This serves as an interesting scenario to apply the close approach toolbox to assess the space-based SDA opportunities. Since the satellites destined for GEO are often high mass and high value, we are also interested in using the close approach toolbox to gain insight into the threat landscape that exists, via observation window analysis. To achieve this, we will first discuss how we modelled the MEV-2 EP transfer orbit. We will then present a model template of a potential close approach RPO manoeuvre. Finally, we apply ANCAS to the MEV-2 EP transfer orbit to identify potential SDA opportunities and threat windows.

### 6.1 Q-Law

To model the MEV-2 EP orbit we implement a trajectory formation algorithm known as Q-Law, first established by Petropoulos [8, 9]. The Q function is a proximity quotient: quantifying in terms of scaling functions, a measure of the relative closeness between the current spacecraft state and the selected target state. The units are that of time-squared, so can be conceptually thought of as a time-to-intersection of states. The Q-law works by selecting the thrust pointing vector at each integration time step which minimises the Q function most rapidly. It is incorporated within the equations of motion for a spacecraft and manifests itself as an additional force perturbation term applied at each integration time step, hence the term closed loop control law. The classical Q-law candidate Lyapunov function is defined as:

$$Q = (1 + W_P P) \sum_{æ} W_{æ} S_{æ} \left[\frac{\Delta(æ, æ_\Gamma)}{\dot{æ}}\right]^2, \qquad (10)$$

where æ = [a, e, i, ω, Ω].

The five slow classical elements (æ) are semi-major axis, a; eccentricity, e; inclination, i; argument of periapsis, ω; and longitude of ascending node, Ω. $W_P$ and $W_{æ}$ refer to positive weight constants, which control the relative rate of convergence to corresponding target orbital element; $æ_\Gamma$ defines the target orbital state; and $\dot{æ}$ is the maximum rate of change of each orbital element with respect to true anomaly and thrust direction. $S_{æ}$ is a scaling function to ensure convergence, taking the form

$$S_{æ} = \begin{cases} \left[1 + \left|\frac{a - a_\Gamma}{m a_\Gamma}\right|^n\right]^{\frac{1}{r}}, & æ = a \\ 1, & æ = e, i, \omega, \Omega, \end{cases} \qquad (11)$$

where m, n and r are positive scalars; $\Delta(æ, æ_\Gamma)$, defines a distance metric function between the instantaneous and target state of the form

$$\Delta(æ, æ_\Gamma) = \begin{cases} cos^{-1}[cos(æ - æ_\Gamma)], & æ = \omega, \Omega \\ æ - æ_\Gamma, & æ = a, e, i; \end{cases} \qquad (12)$$

Finally, to ensure trajectories do not pass through the Earth, a penalty function, P, is added to enforce a minimum-periapsis-radius constraint

$$P = exp[k(1 - \frac{r_p}{r_p^*})], \quad (13)$$

where $r_p$ is the osculating periapsis radius and $r_p^*$ is a lower bound on $r_p$, $k$ is positive scalar.

To ensure the proximity quotient $Q$tends to 0 at a maximum rate, the derivative of the proximity quotient, $\dot{Q}$ must be minimised. An expression for $\dot{Q}$ is given in terms of its partial derivatives, giving

$$\dot{Q} = \sum_{æ} \frac{\partial Q}{\partial æ} \dot{æ} \quad (14)$$

which can be redefined in the RSOs in-plane ($\alpha$) and out-of-plane ($\beta$) angle as follows

$$\dot{Q} = \psi_1 cos\beta\ sin\alpha + \psi_2 cos\beta\ cos\alpha + \psi_3 sin\beta \quad (15)$$

with the non-trigonometric terms expressed in terms of the partial derivatives, $\frac{\partial Q}{\partial æ}$ . These analytic expressions are calculated using the symbolic toolbox in Matlab[10].

We now apply a non-linear least square fitting procedure to estimate the Q-law weighting parameters and average thrust magnitude that best fits the MEV-2 data. The TLEs published by Space-Track.org during the period of the orbital transition were used to construct residual functions to minimise. In Fig. 8a and 8b we show the results of the transfer ephemeris in Earth-Centred Inertial (ECI) coordinates and the non-linear least squares fit of the orbital elements using the Q-law EP model. The computed Q-Law weighting parameters for the MEV-2 mission are given in Table 3 accompanied by the associated details of the transfer.

| | |
|---|---|
| Initial state: (a, e, i) | (26582, 0.590, 3.89) |
| Target state : (a, e, i) | (41897, 0.032, 0.11) |
| Transit time: (days) | 153.41 |
| Q-Law parameters: Wæ | (4.03, 2.81, 8.45,0,0) |
| Integrator parameters: | VCABM |
| Spacecraft parameters: (T, m, ISP) | (0.031, 2495, 2000) |
| Epoch: | 26/08/2020 |

*Table 3: Modelled MEV-2 EP transfer scenario parameters*

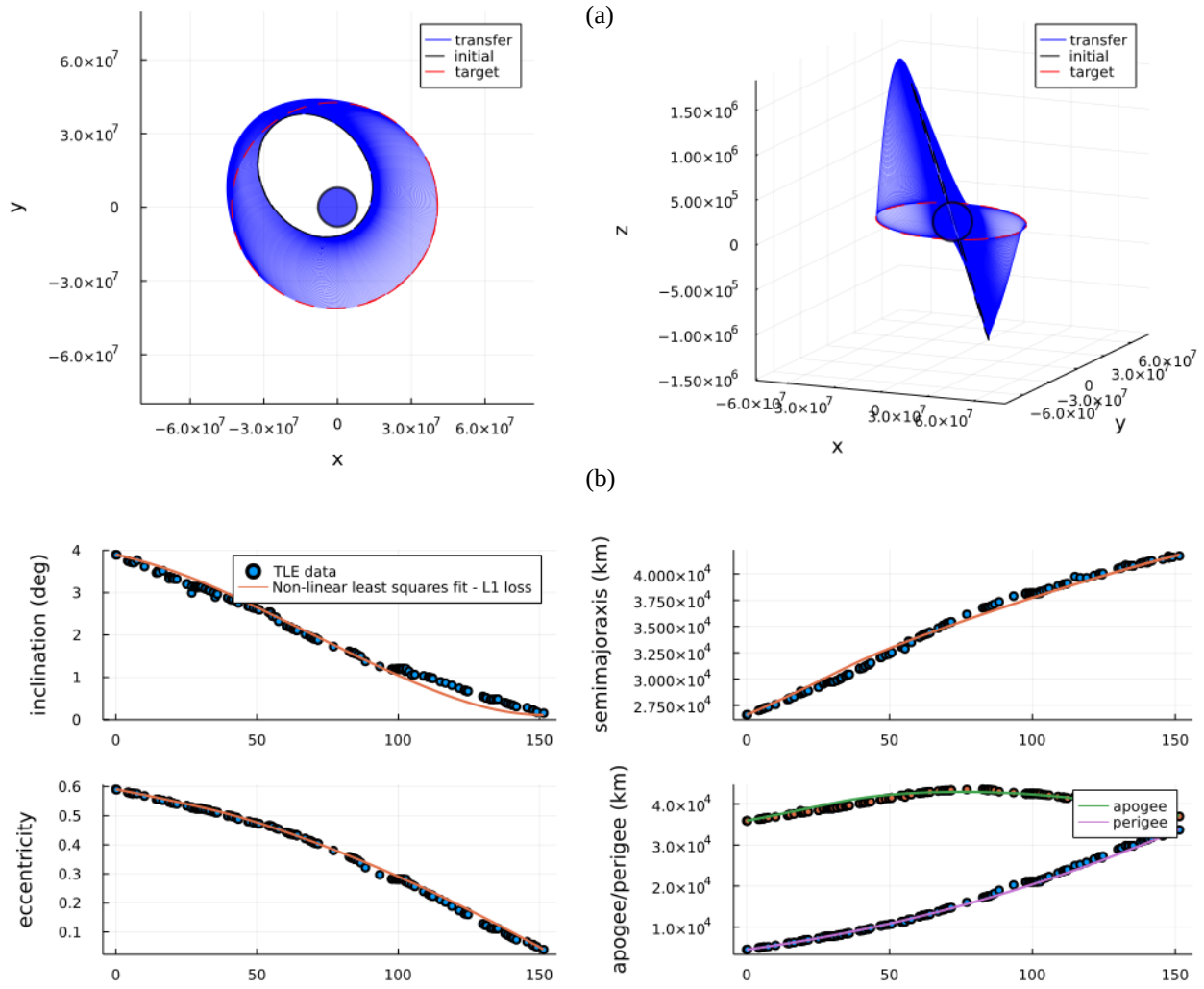


*Fig. 8: MEV-2 modelled trajectory (a) ECI ephemeris (b) inclination, semi-major axis, eccentricity and apogee/perigee histories*

### 6.2 Close Proximity Operations

Once the Q-Law trajectory has reached its approximate target orbit, we have the ability to incorporate a close approach RPO option. The RPO modelling work is the subject of an ongoing investigation into threat mitigation strategies. In particular, we aim to assess the feasibility of an unfriendly satellite perfoming circumnavigation inspections of the spacecraft, either during its final phase of the EP GEO transfer or at lower altitudes. If there is an opportunity to do so, the close approach threat warning could help in determining the timings of these events so that suitable preparation for mitigation is possible.

In Fig. 9 we present a template for a possible RPO approach of a target in a circular orbit. During the RPO, the spacecraft first enters a holding ellipse before performing a Sun-following manoeuvre around its target. The Sun-

following manoeuvre provides the spacecraft with optimal lighting conditions for imaging its target by keeping the spacecraft at a fixed distance on the target-Sun vector.

In Fig. 9 (d), we show how the combined dV expenditure varies with target altitude. This template was applied to LEO target altitudes, but the same methods can be applied to GEO. Further work is needed to generalise this analysis to all phases of the GTO-GEO, but there is potential to use this work to identify feasible opportunities for circumnavigation operations targeting MEV-2 based on dV limitations.

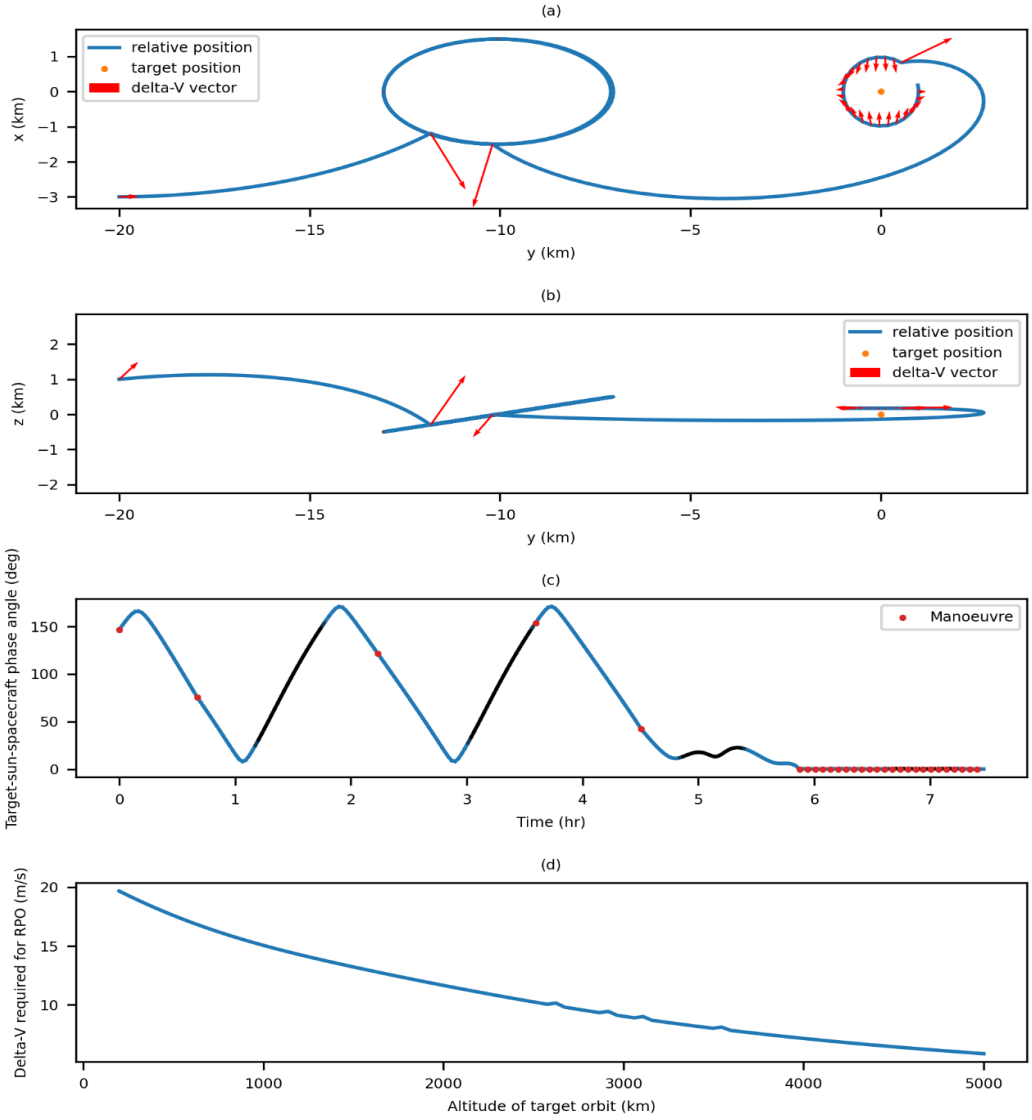


*Fig.9: A potential RPO approach involving a holding ellipse and a Sun-following manoeuvre around a target located at 1200km altitude. Viewed in the Clohessey-Wiltshire xy plane with thrusting vectors shown (a). Viewed in the Clohessey-Wiltshire yz plane with thrusting vectors shown (b). The phase angle between the target, sun and spacecraft over the duration of the RPO (c). The total dV required to perform the RPO at various altitudes (d). Note that the phase angle is approximately zero during the Sun-following manoeuvre and that the plotted line becomes black as the spacecraft passes into the Earth's umbra.*

### 6.3 EP Transfer Close Approach Assessment

We now present the results of applying the full ephemeris spanning 153 days of the modelled MEV-2 orbital transfer to population scenario 2. In order to reduce computational burden, the scenario processes all the non-debris (as defined in the Future Populations dataset) objects with mass > 4kg, eccentricity < 0.9 and perigee > 1000, giving a total population size of 10010. Note, the mass limit was chosen to reflect, the smallest expected spacecraft in the GEO regime.

In Fig. 10a we plot the period of the objects with a close approach within a 200km range for the 153 day timespan of the EP transfer; noting that a period of 1 day corresponds to a GEO object. The highly eccentric initial GTO orbit of MEV-2 means the close approaches to the GEO population occur repeatedly throughout the transfer. We also observe Medium Earth Orbit (MEO) and Highly Eccentric Orbits (HEO) or GTO orbit interactions, mostly with periods between 0.1 and 0.6 days, these reduce in frequency throughout the transfer. The close approaches detected at the end phase with periods <0.8 days most likely correspond to highly eccentric orbits because it is known that MEV-2 is almost fully circularised (~1 day period) at this stage: HEO/GTO, with apogee near GEO altitudes would have the small periods observed here.

In Fig. 10b and 10c histograms depict the the total number of close approaches per day for D* = 50km and 100km respectively. We see that when D* = 100km (Fig. 10c) there is a significant increase in number of close approaches during the final phase of the GTO-GEO transfer, peaking at about 30 per day. However, for D* = 50km (Fig. 10b) the frequency of close approaches is significantly less and more uniform throughout the simulated period. Overall, if during its EP transfer the spacecraft was tasked with collecting resolved imagery of the deep space population there are evidently numerous SDA opportunites across a diverse range of orbits.

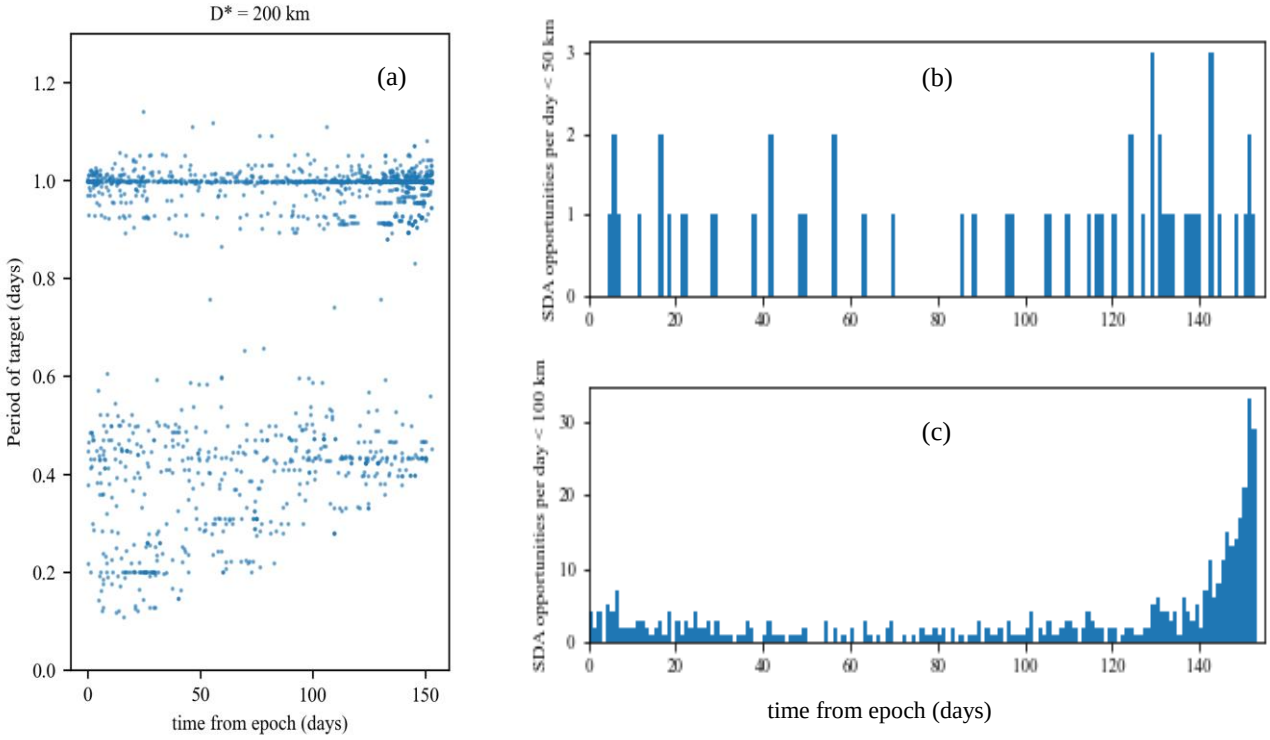


*Figure 10: (a) period of close approach target orbit calculated during MEV-2 orbital transfer; (b-c) number of close approaches per day for (b) D* =50km (c) D* = 100km*

From the threat window perspective, as seen in Fig. 8b the instantaneous apogee of MEV-2 remains close to GEO altitudes throughout the raise, during these times there could be an increased vulnerability to opportunistic RPO inspections from resident GEO spacecraft. As mentioned in the previous section, we are interested in taking the details of these close approaches and modelling circumnavigation scenarios in terms of dV requirements to assess the viability of these potential threat corridors. In terms of tractability, we note that we have taken a near complete deep space population of satellites not all of which will neccessarily pose a threat, so the majority of these close approaches will not need to be analysed.

## 7 CONCLUSIONS AND FUTURE WORK

In this paper, we have applied modelling, simulation and optimisation routines to explore a broad set of questions pertaining to close approach interactions between an orbit (or constellation) of interest and an RSO population.
Firstly, we investigated the orbital configurations that maximise possible SDA opportunities across a LEO target population. Notably, by comparing the target population density with the close approach statistics we have shown that direct correlations exist in the space-based sensor's semi-major axis variable but not in inclination. We have seen that a local maximum in SDA opportunities occur when a space-based sensor is positioned in a ~82deg counter direction orbit relative to the target population's densely populated retrograde polar orbits at ~97deg. The large variation in SDA opportunities across the orbital parameters considered here has highlighted the importance in orbit selection for a space-based sensor.

Secondly, a quantitiative assessment of the feasibility of SDA opportunities in terms of the time available to make an observation was made. More work is needed to cover more sensor specific aspects of feasibility, such as the illumination conditions, which is likely to impact the proportion of viable observable targets too, as well as the expected resolution of target based on range and target size. This work has provided the basis for constructing space-based sensor scheduling plans. In future, we aim to construct a cost function: scoring the feasibility calculations, expected image quality and target prioritisation calculations of each close approach. This will enable the investigation of various optimisation routines in an effort to further maximise the utility of space-based sensor systems, past orbital design.

Next, a proof of concept method for constructing constellations of space-based sensors was put forward. Here, we used the orbital assessment calculations to pose a subset selection problem, which was solved using a NSGA-II multi-objective optimiser to obtain a pareto-optimal set of solutions across the target population coverage and total SDA opportunities performance metrics. The comparisons between random constellation selection, and the optimised results, highlight the importance of an informed space-based constellation design. We note that although we showcased an example where we optimised the total SDA opportunities and population coverage metrics across a fairly general RSO population scenario, the tools developed allow for the same optimisation routines to be applied to more specific populations. In future work, the same analysis could be applied to a variety of mega-constellations, to investigate how the Pareto-optimal constellations solutions compare.

A short study was also carried out to investigate the feasibility of a single space-based sensor with manoeuvring capability, tasked with visiting all the orbits of the constellation solutions found. We obtain the best sequence of orbital transfers by solving a minimum dV Travelling Salesman Problem. The results depict a tradeoff in total dV usage with the associated overall population coverage. Notably, we have demonstrated that it is feasible for a single satellite with manoeuvring capability, in time, to achieve comparable population coverage to a static constellation, potentially offering cost saving opportunities for space-based SDA. However, more work is required to verify the results using longer time span simulations, to ensure the unique number of satellites metric is saturated across all candidate orbits. In future work, a Multiple Travelling Salesman approach to this problem could be investigated: considering the case of a small constellation of manoeuvring space-based sensors, not just one.

Our final area of investigation was assessing the close approach interactions experienced by a low thrust EP transfer to GEO. This was tested against a near complete deep space population. In future work, more detailed analysis could be carried out against a more relevant catalogue of space objects, and also further develop the capability to assess the

threat landscape of a wider range of EP missions; with the aim of potentially providing earlier warnings of heightened risk to spacecraft with complex orbital dynamics. In addition, the feasibility of resident GEO spacecraft making opportunistic RPO inspections of a low-thrust manoeuvring target during different phases of its orbital transfer could be investigated. The combination of close approach calculations, state estimation and manoeuvring dynamics offers an opportunity to further develop threat modelling capability.

In future work, more detailed analysis could be undertaken to repeat the analysis above adopting a more accurate TCA algorithm, with a SGP4 semi-analytical propagator accompanied with a covariance propagation model, taking a more specific TLE population of interest, and simulating over a longer timespan. This will provide validation of the findings and enable a more detailed analysis of feasibility: moving this work beyond proof of concept.

## REFERENCES


1. Vallado, D.A., *Fundamentals of astrodynamics and applications*. Vol. 12. 2001: Springer Science & Business Media.
2. Alfano, S. and D. NEGRON, *Determining satellite close approaches.* Journal of the Astronautical Sciences, 1993. **41**(2): p. 217-225.
3. Denenberg, E., *Satellite closest approach calculation through Chebyshev Proxy Polynomials.* Acta Astronautica, 2020. **170**: p. 55-65.
4. Denenberg, E. and P. Gurfil, *Improvements to time of closest approach calculation.* Journal of Guidance, Control, and Dynamics, 2016. **39**(9): p. 1967-1979.
5. Deb, K., et al., *A fast and elitist multiobjective genetic algorithm: NSGA-II.* IEEE transactions on evolutionary computation, 2002. **6**(2): p. 182-197.
6. Samui, P., S.S. Roy, and V.E. Balas, *Handbook of neural computation*. 2017: Academic Press.
7. George, S., et al. *Phantom Echoes 2: A Five-Eyes SDA Experiment on GEO Proximity Operations*. in *Proc 22nd AMOS Conf*. 2021.
8. Petropoulos, A.E., *Refinements to the Q-law for the low-thrust orbit transfers.* 2005.
9. Petropoulos, A.E., et al., *Techniques for designing many-revolution electric-propulsion trajectories.* Advances in the Astronautical Sciences, 2014. **152**(3): p. 2367-2386.
10. Toolbox, S.M., *Matlab*. Mathworks Inc, 1993.